Journal of Colloid and Interface Science 666 (2024) 629–638

Contents lists available at ScienceDirect

Journal of Colloid And Interface Science

journal homepage: www.elsevier.com/locate/jcis

Nanoantennas report dissipative assembly in oscillatory electric fields

Hong Wei [a,e,1,2], Héctor Pascual-Herrero [a,e,1], Serxho Selmani [b,e], Sebastian Marroquin [a,e], Gabriel D. Reginato [a,e], Zhibin Guan [a,b,c,d,e], Regina Ragan [a,c,e,*]

[a] Department of Materials Science and Engineering, University of California, Irvine, Irvine, CA 92697-2585, United States
[b] Department of Chemistry, University of California, Irvine, Irvine, CA 92697-2025, United States
[c] Department of Chemical and Biomolecular Engineering, University of California, Irvine, Irvine, CA 92697-2580, United States
[d] Department of Biomedical Engineering, University of California, Irvine, Irvine, CA 92697-2715, United States
[e] Center for Complex and Active Materials, University of California, Irvine, Irvine, CA 92697, United States

GRAPHICAL ABSTRACT

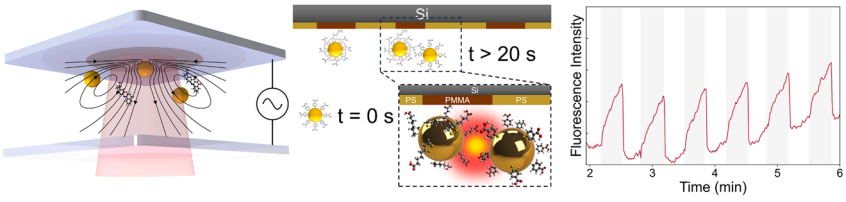

ARTICLE INFO

Keywords:
Electrohydrodynamic flow
Dissipative assembly
Metal enhanced fluorescence
Surface enhanced Raman scattering
Fluorescence microscopy

ABSTRACT

Understanding driving forces for dissipative, i.e., out of equilibrium, assembly of nanoparticles from colloidal solution at liquid–solid interfaces provides the ability to design external cues for reconfigurable device response. Here electrohydrodynamic flow (EHD) at an electrode-liquid interface is investigated as a dissipative driving force for tuning optical response. EHD results from an oscillatory electric field in a liquid cell between two electrodes and drives assembly of gold nanoparticles (NP) into two-dimensional clusters on electrode surfaces. Clusters are chemically crosslinked during assembly to freeze assemblies for electron microscopy characterization in order to understand how to 'nucleate' cluster formation. Electron microscopy images show deposition with a potential having an amplitude of 5 V and frequency of 100 Hz produces surfaces with isolated NP, which can seed EHD flow. A second deposition step at 5 V and 500 Hz produces a high density of quadramers on surfaces. When exciting near the local surface plasmon resonance of the Au NP clusters formed during assembly, Au NPs serve as *in situ* nanoantenna reporters of assembly and disassembly. Surface enhanced Raman scattering (SERS) measurements of Au NP capped with 4-mercaptobenzoic acid show order of magnitude signal

Abbreviations: Au NP, gold nanoparticles; Ag NP, silver nanoparticles, SEM, scanning electron microscope; CBS, concentric backscatter detector; LSPR, localized plasmon resonance; MEF, metal enhanced fluorescence; SERS, surface enhanced Raman scattering; EHD, electrohydrodynamic; 4-MBA, 4-mercaptobenzoic acid; ITO, indium tin oxide; IPA, isopropyl alcohol; DI, deionized water; DMSO, dimethyl sulfoxide; EDC, 1-Ethyl-3-(3-dimethyl aminopropyl) carbodiimide; s-NHS, N-hydroxysulfosuccinimide; MES, 2-[N-morpholino] ethanesulfonic acid; APTES, 3-(aminopropyl) triethoxysilane; PMMA, poly methyl methacrylate; PS, poly styrene; AC, alternating current.

* Corresponding author at: Department of Materials Science and Engineering, University of California, Irvine, Irvine, CA 92697-2585, United States.
E-mail addresses: hwei7@uci.edu (H. Wei), hpascua1@uci.edu (H. Pascual-Herrero), serxhoselmani@gmail.com (S. Selmani), samarroq@uci.edu (S. Marroquin), greginat@uci.edu (G.D. Reginato), zguan@uci.edu (Z. Guan), rragan@uci.edu (R. Ragan).
[1] These authors contributed equally.
[2] Current location: Process Research & Development, Merck & Co., Inc., West Point, PA, 19486, United States.

https://doi.org/10.1016/j.jcis.2024.03.203
Received 17 November 2023; Received in revised form 15 March 2024; Accepted 30 March 2024
Available online 9 April 2024

enhancements occur during cluster formation in the presence of an oscillatory field, which occurs on a time scale of seconds. Confocal fluorescence spectroscopy is used to monitor the dissipative assembly of Au NP over multiple cycles. Results provide insight on how electrical stimuli and seeding local perturbations affects formation of NP clusters and resultant optical response provides insight on how to tune response of optically active surfaces.

1. Introduction

Self-assembly of optically active materials from nanoparticle building blocks in colloidal solution relies on the ability of directing interactions between nanoparticles (NP) using a wide parameter space. Design of reconfigurable surfaces is available via electrostatic interactions, chemical, and external electromagnetic forces [1–7]. For example, optical forces in combination of electrostatic interactions have initiated dissipative assembly of chains of NP along the polarization axis of an optical beam [6] and light driven assembly of polymer colloidal spheres resulted in dynamic assembly and disassembly of 2-dimensional clusters [5] and spinning microgears [3]. While colloidal systems offer the ability to mimic molecular assembly for imparting novel functionality [8], further understanding how electrical, osmotic, hydrodynamic and phoretic driving forces to tune interactions to produce active colloids is needed [9]. In particular, understanding electric stimuli as a driving force for dissipative assembly of NP with resonances at optical frequencies can produce reconfigurable metasurfaces. Dynamic assembly of plasmonic NP with resonances at optical frequencies has been used to change absorbance and reflectance on surfaces using electrostatic forces [10,11]. Electrotunable systems using functionalized Au NP can use small voltage pulses to tune between window and mirror states [12]. Furthermore, rich 2D phase behavior with varying electric field strength is observed when NP are confined between electrodes separated by distances a few orders of magnitude larger than the nanoparticle's diameter [13]. Electrokinetic phenomenon including electrohydrodynamic (EHD) flow and AC-induced charge electroosmosis, resulting from an applied oscillatory potential, can drive lateral assembly of NP in response to an electric field gradient on an electrode-liquid interface [1,2,14–17]. EHD flow is a dissipative driving force [14,18,19], where assemblies may disassemble if the electrical stimuli is not maintained. Dissipative assembly of micron scale particles using EHD flow has been studied extensively [13,14,16,20], where fluid dynamics can be approximated with the Stokes equations [21]; whereas EHD flow for assembly of NP remains relatively much less explored [2,15,22], with few reports on dissipative assembly of NP using chemical fuels rather than electrical stimuli studied here [23]. EHD driving forces represent a path for large-scale manufacturing of low-cost optoelectronic devices, including sensors and photovoltaics [24].

Driving forces for inducing EHD flow under an oscillatory potential for assembly of Au NP confined in a liquid cell is investigated here. The *2-dimensional* clusters of Au NP formed as a result of EHD flow are chemically crosslinked for electron microscopy analysis to determine the frequency regime to generate nucleation sites for EHD flow and frequency regime for lateral assembly leading to cluster growth. As colloidal NP are typically stabilized via electrostatic repulsion, chemical crosslinking in solution will normally lead to uncontrolled aggregation. EHD flow is confined to the working electrode surface and thus mitigates aggregation in bulk solution. Dissipative assembly on surfaces with isolated Au NP serving as nucleation seeds in aqueous solution is then monitored using surface enhanced Raman scattering (SERS) and fluorescence microscopy using the identified deposition parameters leading to lateral assembly. The resultant electromagnetic field enhancement, associated with excitation of the LSPR of plasmonic NP as they are assembled into clusters, is used to monitor assembly *in situ*. SERS spectra of Au NP functionalized with 4-mercaptobenzoic acid (4-MBA), as reporter molecules, show the SERS signal saturates on a time scale of 20 s. Fluorescence microscopy probes dissipative assembly by monitoring emission intensity in the presence or absence of the oscillatory field. *In situ* fluorescence studies show that increases and decreases in fluorescence intensity are correlated with turning on and off the external electric stimuli and thus able to report dissipative assembly of Au NP.

2. Materials and methods

2.1. Electrode Materials

The working electrode is composed of P-type, boron doped, (1 0 0) silicon wafers (University Wafer, USA) with resistivity of 0.001–0.005 ohm-cm. Silicon wafers are cleaned for 5 min by 20% v/v hydrofluoric acid (HF, Fisher Scientific, USA) in deionized (DI) water with resistivity of 18.2 MΩ cm^{-1}, obtained from a Milli-Q Millipore System and then immersed in DI water to regrow a thin silicon dioxide layer. *The potential of HF to cause severe injury mandates extreme caution during usage.* In order to form chemically patterned templates, solutions of 1 wt% random copolymer Poly(styrene-*co*-methyl methacrylate)-α-Hydroxyl-ω-Tempo moiety (PS-r-PMMA) (M_n = 7400, M_w = 11800, M_w/M_n = 1.60, Polystyrene content: 59.6 mol%, Polymer Source, Inc., Canada) in toluene (Fisher Scientific, USA) are spin coated on Si wafers at 3000 rpm for 45 s, annealed under vacuum at 170 °C for 48 hr, and then rinsed with toluene to leave a brush layer. Diblock copolymer poly(styrene-*b*-methyl methacrylate) (PS-*b*-PMMA) (Mn S-*b*-MMA 170000-*b*-145000 g mol^{-1}) (Polymer Source, Inc., Canada) is spin coated at 5000 rpm for 45 s and then annealed for 72 hr at 170 °C.

In the case of fluorescence imaging, Si wafers are functionalized with 3-(aminopropyl) triethoxysilane (APTES) to avoid fluorescence background from the polymer. Si wafers are first immersed in 3:1 H_2SO_4:H_2O_2 (piranha solution) at room temperature for 30 s in order to hydroxylate the surface, and functionalized with amine group by soaking in a solution of 2% APTES in toluene and baked on a hotplate at 110 °C for 30 min. *The potential of piranha solution to cause severe injury mandates extreme caution during usage.* ITO coated glass slides, with sheet resistance of 70–100 ohm cm^{-1} (Delta Technologies, USA), are used as the counter electrode. ITO slides are cleaned by rinsing with ethanol, isopropyl alcohol (IPA), and DI water and then dried by N_2. Indium wire (Chip Quik, Canada) is used for electrical contact by soldering to surfaces. APTES, DMSO, ethanol, and IPA were purchased from Sigma Aldrich (USA).

2.2. Experimental setup

A schematic of the experimental setup for *in situ* monitoring of EHD driven dissipative assembly of Au NP is shown in Scheme 1. A Si substrate, serving as a working electrode, and an optically transparent indium tin oxide (ITO) coated glass slide, serving as a counter electrode, are assembled in a liquid cell using a 90 μm spacer layer (9816L, 3M, USA). Before assembly, PMMA domains on PS-*b*-PMMA/Si are immersed in dimethyl sulfoxide (DMSO) for 5 min and then 5 vol% ethylenediamine in DMSO for 5 min in order to functionalize the PMMA regions with amine groups for coupling to Au NP [2]. Our previous work shows lipoic acid functionalized Au NP will preferentially deposit on the PMMA domains [25]. Au NP, functionalized with lipoic acid, with a diameter of 40 nm, are purchased from Nanocomposix (USA). After concentrating the NP solution and dispersing it in deionized water, the zeta potential was measured to be −53 mV using a Zetasizer Nano ZS Instrument (Malvern Panalytical, U.K.). In the liquid cell, 2 μL of 20 mM

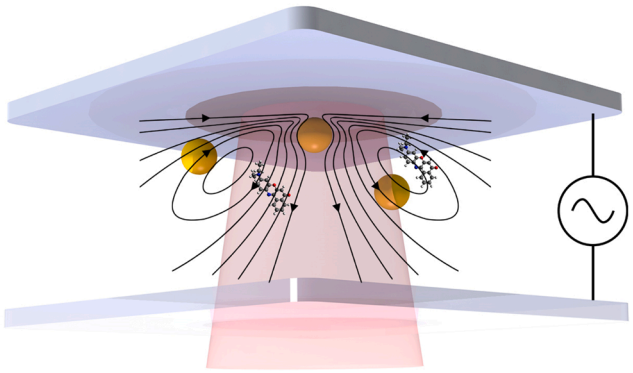

Scheme 1. Schematic of liquid cell for assembly of Au NP in oscillatory electric field: An oscillatory potential between a Si substrate (top) and ITO coated glass slide (bottom) is applied to drive EHD flow of Au NP. The transparent ITO allows for *in situ* fluorescence imaging and SERS vibrational spectroscopy.

N-hydroxysulfosuccinimide (s-NHS) in 0.1 M 2-[N-morpholino] ethanesulfonic acid (MES) buffer (pH of 4.7) is added to 0.25 mL of a solution of 1.3 nM lipoic acid functionalized Au NP. This is followed by adding 2 μL of 8 mM 1-Ethyl-3-(3-dimethyl aminopropyl) carbodiimide (EDC) in 0.1 M MES buffer to the s-NHS/NP solution. All solutions are freshly prepared before assembly of the liquid cell and the pH of the final solution was measured to be 5.3. Ag NP, functionalized with lipoic acid, with a diameter of 50 nm, are purchased from Nanocomposix (USA). Ag NP are dispersed in deionized water to achieve a concentration of 1.3 nM. In the liquid cell, s-NHS and EDC in MES buffer solutions are added following the same order and volume ratio as for Au NP.

The absorbance spectrum of the colloid has a maximum value at 523 nm, as provided by the manufacturer. Our previous work has shown the localized surface plasmon resonance (LSPR) will red shift when forming clusters with the degree of the redshift being dependent on the gap spacing between clusters [1]. Au NP with a diameter of 40 nm were chosen, as our previous work has shown that deposition of NP with smaller diameter are more heavily influenced by Brownian motion than EHD flow at room temperature [2]. EDC, ethylenediamine, s-NHS and MES buffer were purchased from Sigma Aldrich (USA).

After assembling the liquid cell, EHD assembly is conducted using an oscillatory electric field with varying frequency. For single deposition, a potential with an amplitude of 5 V is applied across electrodes for 2 min and the frequency is varied as follows: 100 Hz, 500 Hz, 1000 Hz and 1500 Hz. In the case of two-step deposition, an oscillatory potential with amplitude of 5 V and frequency of 100 Hz is applied for 2 min. This is followed by a second deposition step that is conducted with the same oscillatory potential with the frequency varied between 500 and 1500 Hz for another 2 min. After depositions, the liquid cell is dismantled and the silicon surface is thoroughly rinsed with deionized water and IPA and then dried with N_2 for further characterization.

2.3. Characterization

Electron microscopy images on the samples were acquired by a FEI Magellan (Thermo Fisher Scientific, USA) scanning electron microscope (SEM). SEM images with secondary electrons were acquired using a voltage of 25 kV, a current of 25 pA, a dwell time of 30 μs, and a 4 mm working distance. Images acquired with a retractable concentric backscatter detector (CBS) used a voltage of 10 kV, a current of 100 pA, a dwell time of 30 μs, and 8 mm working distance, without a stage bias. For confocal fluorescence microscopy, Au NP functionalized with lipoic acid ligands were deposited on Si functionalized with APTES to eliminate fluorescence background from the diblock copolymer. An oscillatory potential with amplitude of 5 V and frequency of 100 Hz for 2 min with EDC and s-NHS, is used; the same conditions as on the PS-*b*-PMMA surface. The Si electrode and Au NP seeds were coated with amorphous carbon with a thickness of approximately 5 nm using an EM ACE 600 high vacuum sputter coater (Leica Microsystems, Germany). Then the Si and ITO electrodes were assembled into liquid cells in a capacitor architecture using a 25 μm adhesive spacer layer (3M, USA). Confocal fluorescence microscopy is performed using a Zeiss LSM 780 confocal microscope (Zeiss, Germany) at laser excitation wavelength of 561 nm and with LD C-Apochromat 63x/1.15W Korr M27 lens, which has a free working distance of 600 μm. In the microfluidic channel, the solution was composed of 8 μL of an aqueous solution of 0.5 mM nile red (Acros Organics, USA) fluorophore and 150 μL of 1.3 nM Au NP. Dynamic imaging was performed with an applied oscillatory potential with amplitude of 5 V and a frequency of 500 Hz was held on for 20 s and off for 20 s for 12 cycles in total, while exciting the sample through the ITO coated slide with a 561 nm laser continuously.

In situ SERS spectral imaging is performed by an i-Raman Plus Portable Raman Spectrometer (BWTEK, USA) at an excitation wavelength of 785 nm, power of 34 mW, spectral resolution of 4.5 cm^{-1}, 0.22 N_A, and 1 s integration time. The laser spot size is 80 μm at the focal plane on the Si electrode. Assembly of NP clusters is monitored between lipoic acid functionalized Au NP seeds, deposited using an oscillatory potential amplitude of 5 V and a frequency of 100 Hz for 1 min with EDC and s-NHS as described above, and 4-mercaptobenzoic acid (4-MBA) functionalized Au NP assembled using an oscillatory potential amplitude of 5 V and a frequency of 500 Hz in the second deposition step. Functionalization of citrate stabilized Au NP (Nanocomposix, USA) with 4-MBA (Sigma Aldrich, USA) is performed by mixing 12 mL of 0.13 nM citrate stabilized Au NP with 16 μL of 0.1 M K_2CO_3 and centrifuging for 30 min at 1.7 RCF. The solution is resuspended in a basic solution of NaOH diluted in DI water to have a pH of 11.7 and 12 μL of 10 mM 4-MBA in ethanol is added to the Au NP solution. The solution is continuously stirred overnight and then centrifuged for 30 min at 1.7 RCF to remove excess of 4-MBA before dispersing in DI water. In the second deposition step, the liquid cell is reassembled and filled with a 1.3 nM solution of 4-MBA functionalized Au NP with a 90 μm spacer layer, separating an ITO electrode on the bottom and the PS-*b*-PMMA coated Si electrode with Au NP seeds on the top. SERS spectra was acquired during the second deposition every 5 s and was processed using an asymmetric least square correction for baseline correction, and a Savitzky-Golay filter for data smoothing. All spectra were normalized by setting the vibrational band at 520 cm^{-1} from the Si substrate to a value of 1.

3. Results and discussion

3.1. Dependence of cluster size on oscillatory field frequency

An oscillatory electric field is applied across the liquid cell containing 1.3 nM aqueous solution of lipoic acid functionalized Au NP between Si and ITO electrodes, previously shown in Scheme 1. The Si working electrode is coated with a PS-*b*-PMMA thin film (Scheme 2). The presence of amine-functionalized PMMA lamellar domains with approximate width of 40 nm on the diblock copolymer template, shown in the atomic force microscopy image Fig. S1, aids in dispersing Au NP across the surface. Au NP selectively attach to functionalized PMMA domains using carbodiimide crosslinking chemistry as demonstrated in our previous work [1,2,25]. When applying an oscillatory potential, forces on NP that direct their motion with respect to electrode surfaces include electrophoresis, dielectrophoresis and EHD flow [15,22]. In the case of electrophoresis, Au NP will experience force along the applied electric field, normal to the electrode surface, illustrated in Scheme 2a. In Scheme 2b, EHD flow can result from the local perturbation of free charge distribution at the liquid electrode interface caused by the deposition of a Au nanoparticle on a PMMA domain [16,26–27] leading to lateral assembly of Au NP from solution.

Crosslinking chemistry on PMMA domains on Si electrode surfaces [1,25] and between Au NP [2] also serves as a means to 'freeze' clusters,

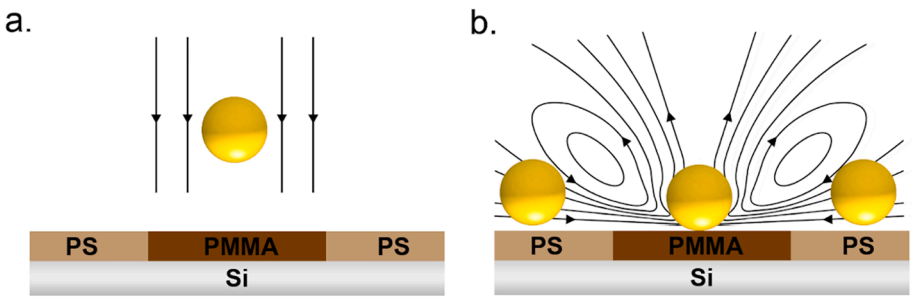

Scheme 2. Schematic of driving forces during deposition of Au NP in colloidal solution on a PS-*b*-PMMA coated silicon substrate in an oscillatory electric field: Au NP deposition when the oscillatory electric field is in the frequency regime where **a)** electrophoretic forces or **b)** EHD flow dominate assembly. PMMA domains are functionalized with ethylenediamine to allow for chemical crosslinking with EDC/s-NHS-activated lipoic acid-functionalized AuNPs. The surface coverage of PMMA is approximately 26% as determined from atomic force microscopy images.

i.e., avoid disassembly when the oscillatory potential is removed and when rinsing the sample before further characterization. Scanning electron microscopy (SEM) images were acquired on the Si working electrode after NP deposition with an oscillatory potential having an amplitude of 5 V and with the frequency varied between 100 and 1500 Hz in order to investigate how the frequency of the oscillatory field affects the influence of electrophoresis versus EHD flow on assembly. Fig. 1a–d shows representative SEM images when the deposition is performed with frequencies of 100 Hz, 500 Hz, 1000 Hz and 1500 Hz, respectively. Examination of the images shows that the average cluster size increases as the frequency of the oscillatory potential increases. Statistical analysis of SEM images, using a minimum of five images with surface area of 30.4 μm^2, was performed for each frequency to determine how frequency affects the number of Au NP in a cluster. The number of clusters (N_n) with a specific number (n) of NP on surfaces is determined via image analysis using Wolfram Mathematica(™). Different clusters are differentiated from one another when the NP are separated by a distance greater than 4 nm (Fig. S2). The percent areal coverage of a particular cluster size for different frequencies, shown in Fig. 1e–h, is calculated as $N_n \times n\pi r^2/A$, where A is the total surface area examined, as the structures most abundant on the surface in the optical beam will have the greatest influence on the measurement.

Deposition at a frequency of 100 Hz leads to primarily isolated NP (referred to as monomers), as observed in Fig. 1a; the percent areal coverage of monomers is nearly twice as large as any other cluster size, shown in Fig. 1e. Thus, the data indicates that electrophoresis is the main driving force for assembly at low frequencies consistent with prior observations [22]. When deposition is performed at 500 Hz, the predominant cluster size is a trimer (Fig. 1f). As the deposition frequency is increased to 1000 Hz and 1500 Hz, the statistical analysis, shown in Figs. 1g and 3h, respectively, shows that the dominant cluster size is a pentamer and larger clusters, size greater than 10, begin to form at more appreciable levels. While a pentamer is most frequently observed at 1500 Hz, there is a large standard deviation (1σ). The average cluster size is calculated to be 1.49 ± 0.15, 3.19 ± 0.77, 4.45 ± 0.52, and 5.30 ± 2.09 for 100 Hz, 500 Hz, 1000 Hz, and 1500 Hz, respectively. Overall, at 1000 Hz and 1500 Hz, EHD flow appears to be the dominate driving force during assembly; it appears that once a Au NP seed is anchored on a PMMA domain, causing a local perturbation of the working electrode potential, when further NP assembly proceeds via EHD flow it will lead to the growth of clusters. It is interesting to note that though the mean cluster size increases with higher frequency the surface area density of NP remains approximately the same, except for the case of deposition at 500 Hz. The number of NP per square micron is calculated as 28.0 ± 2.6, 41.4 ± 8.4, 31.2 ± 3.1, and 28.1 ± 8.2 for 100 Hz, 500 Hz, 1000 Hz, and 1500 Hz, respectively. When deposition is performed at 500 Hz, the smaller observed cluster size and increase in NP overall coverage one can infer there are contributions from both electrophoresis, leading to deposition of isolated Au NP serving as nucleation sites, and EHD flow, leading to lateral assembly.

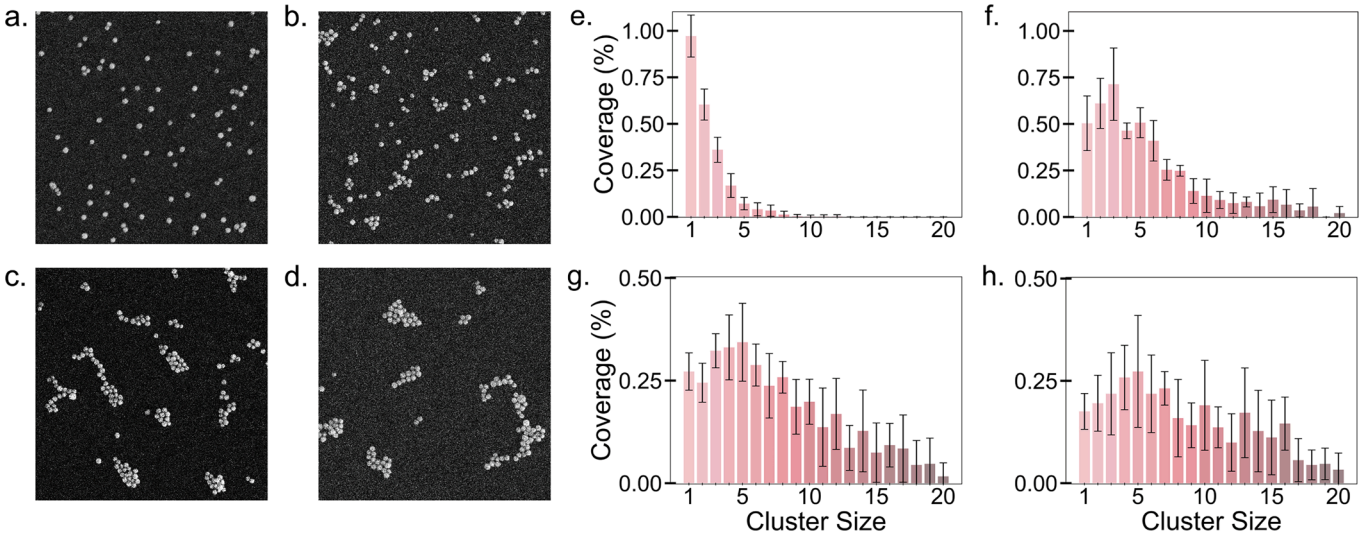

Fig. 1. Representative SEM images of surfaces with a field of view of 2 μm × 2 μm after deposition in the liquid cell for 2 min with an oscillatory potential having an amplitude of 5 V and frequency of a) 100 Hz, b) 500 Hz, c) 1000 Hz, and d) 1500 Hz. e and f) The occurrence of a particular cluster size (N_n) is represented as the percent areal coverage of N_n with respect to the total surface area.

3.2. Designing nucleation sites for EHD flow

Next, a modified deposition process was performed to further investigate the ability to *nucleate* assembly of 2-dimensional clusters via EHD flow using isolated Au NP (monomers) as nuclei for Au NP cluster growth on the Si electrode surface. Based on the above analysis, the investigated frequency where electrophoresis is the primary driving force, leading to mainly monomers on the surface, is 100 Hz at a potential amplitude of 5 V. Thus, these conditions were used for NP deposition for 2 min on a Si working electrode with a PS-*b*-PMMA thin film and ITO as the counter electrode. After the first deposition, the liquid cell is dismantled and a freshly prepared solution of Au NP with EDC and s-NHS in MES buffer is added and the cell is reassembled. Then an oscillatory potential of 5 V is applied with variable frequency; representative SEM images are shown in Fig. 2a–c with frequency of 500 Hz, 1000 Hz, and 1500 Hz, respectively. The two-step deposition process leads to similar surface coverage of NP in all cluster sizes as the single deposition process when performed at the same frequency. The number of NP per square micron after the second deposition is 41.08 ± 11.20 for 500 Hz, 38.22 ± 5.92 for 1000 Hz, and 33.32 ± 3.85 for 1500 Hz. The NP coverage is comparable to that obtained in our previous work when depositing lipoic acid functionalized Au NP using carbodiimide cross-linking chemistry on PS-*b*-PMMA surfaces in the absence of an external field for 40 min [1]. At all investigated frequencies there are more NP on the surface, with respect to a single deposition at 100 Hz, after the second deposition step. Statistical analysis of the percent areal coverage of cluster size under the different deposition conditions was also performed and is shown in Fig. 2d–f. The average cluster size is 3.90 ± 0.97 for 500 Hz, 3.15 ± 0.75 for 1000 Hz, and 6.20 ± 0.78 for 1500 Hz, respectively. The average cluster size also exhibits statistically insignificant changes from the single deposition process when performed at the same frequency.

There are distinct differences that are observed in the two-step deposition with respect to the single deposition process by examining the surface coverage of different cluster sizes shown in Figs. 1 and 2 and the mean number of clusters (N_n) having *n* NP observed in SEM images with a field of view of 30.4 μm^2, shown in Table S1 in Supplemental Materials. For a single deposition process, the number of monomers observed in Table S1 decreases with increasing AC frequency. The two-step deposition has a different trend; when compared with a single deposition, less monomers are observed at a frequency of 500 Hz and more monomers at frequencies of 1000 Hz and 1500 Hz. For the latter two frequencies, the number of clusters in the size range of dimers to pentamers increases significantly in this comparison. The data in Figs. 1 and 2 and Table S1 shows that the total surface coverage of monomers at 500 Hz is decreased to half the value and there is an appreciable increase in the number of clusters of size greater than a hexamer, with respect to the single deposition process. Thus, we can infer that the rate of

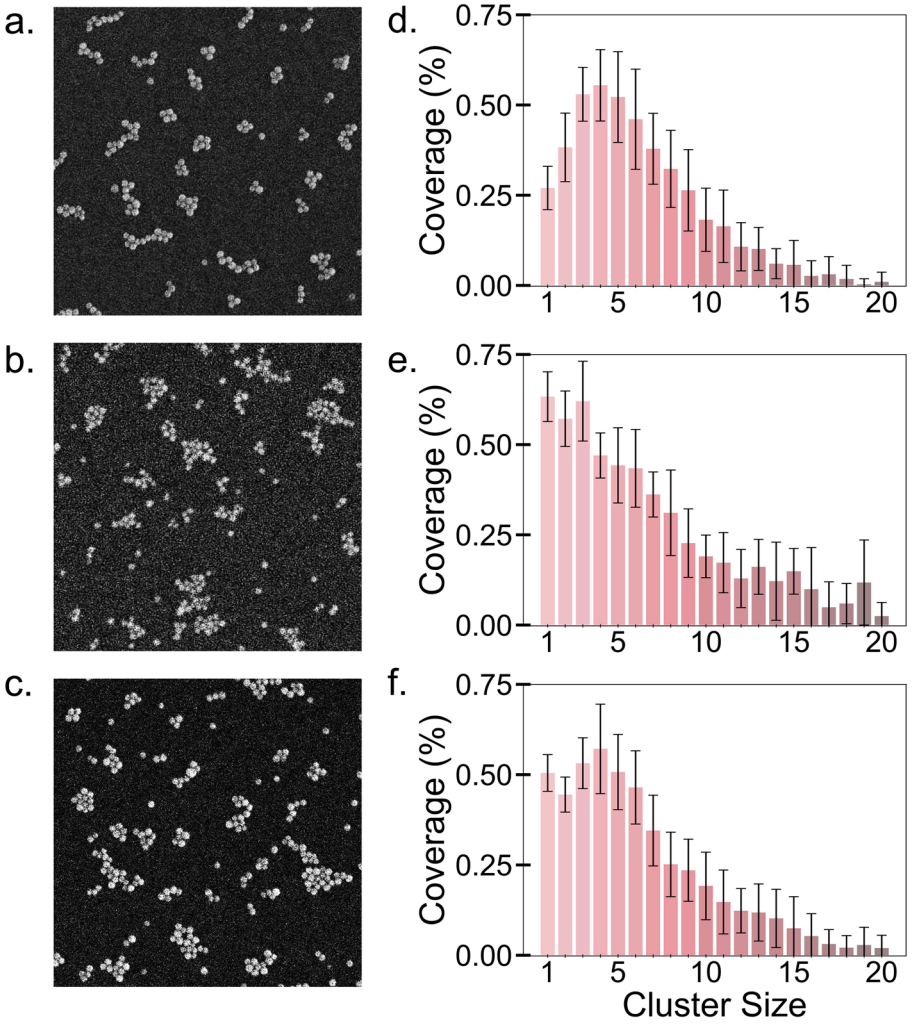

Fig. 2. Representative SEM images of surfaces with a field of view of 2 μm × 2 μm after EHD assembly for 2 min with an oscillatory potential having amplitude of 5 V and frequency of 100 Hz, followed by a second deposition for 2 min at **a)** 500 Hz, **b)** 1000 Hz, and **c)** 1500 Hz with corresponding statistical analysis of percent areal coverage of different cluster sizes is shown in **d, e, f**, respectively.

deposition of monomers to growth of clusters changes in the two-step versus single step deposition processes.

It is not surprising that the surface coverage increases in the second deposition step as compared to the first as the total deposition time increases. Thus, we performed single step depositions at the oscillatory potential amplitude of 5 V at frequencies of 500 Hz and 1500 Hz for 4 min to compare coverage for the same total deposition time. Fig. S4 in Supplementary Materials includes representative SEM images of surfaces with a field of view of 2 μm × 2 μm and statistical analysis of the percent coverage of the different cluster sizes on the surface. It is interesting to note that at 500 Hz, the number of monomers is nearly unchanged with the longer deposition time for a single step deposition whereas the two-step process at the same frequency has half the number of monomers. One can infer that monomers are forming clusters at a rate faster than new monomers are deposited on the surface in the second deposition step. Examining data from single depositions at the frequency of 1500 Hz for both 2 min and 4 min, one observes a similar trend in surface coverage having nearly an equal distribution (within standard deviation) of clusters up to size 9. From Fig. S4 and Table S1, there are significantly more dimers, trimers, quadramers, and pentamers observed in the two-step deposition process versus single depositions at 4 min. There are also statistically less monomers on the surface after single depositions at 4 min than two-step deposition with the second step at 1500 Hz. In this case, one can infer that, as the second deposition progresses, NP have a preference to grow clusters over forming new clusters.

We further investigate how monomers can serve as nuclei for cluster growth in the second deposition step. At the higher frequencies, ≧1000 Hz, it is interesting to note that the number of clusters with size greater than a pentamer decreases more rapidly and there are relatively more monomers on the surface with respect to a single deposition. In order to monitor the preference of cluster formation/growth versus deposition of Au monomers, Fig. 3 shows number of particles (n) in a cluster of a particular size (N_n) normalized to the number of monomers (isolated Au NP) observed on the Si working electrode for both the single deposition and two-step deposition, Fig. 3a and b, respectively. Dashed lines are polynomial fits and are provided as a guide for the eye. Fig. 3a clearly conveys that deposition at 100 Hz (solid circles) produces primarily monomers; 500 Hz (open squares) produces mainly trimers; 1000 Hz (inverted triangles) and 1500 Hz (triangles) have a broader distribution of cluster size. After a two-step deposition process at 500 Hz, Fig. 3b, there is a large increase in n/M with respect to the single deposition process. This observation is consistent with monomers serving as nuclei for EHD flow; the presence of Au monomers serving as seeds appears to tip the balance toward deposition by EHD flow over electrophoresis at this frequency. Depositions at 1000 and 1500 Hz, on the other hand, have relatively less NP in larger clusters than monomers. From Fig. 2e and f, the areal coverage of monomers is shown to approximately double from the single to the two-step deposition process. Thus, the data in Fig. 3b shows that particularly at 1500 Hz, there appears to be a preference for clusters to grow larger versus consuming monomers.

In order to understand the frequency dependence, we examine the origins of EHD flow. Charged colloidal particles, such as Au NP functionalized with lipoic acid ligands used here, near an electrode in the presence of an electric field can alter the body force distribution in the electrode polarization layer, inducing EHD fluid flow. In this case, the electric field near the electrode polarization layer is higher than the bulk field strength and exhibits frequency dependent behavior [22,28]. Numerical studies using the Navier-Stokes equation, in the case of low Reynolds number, with an additional body force to account for free charge in solution, to describe the fluid and particle motion has been derived in detail in many studies [26,29–31]. Flow fields can extend approximately distances 5 times the NP radius, near the surface [26]. At low frequencies ≲ 200 Hz, our observations are consistent with reports that electrophoresis is the dominant driving force [22]. At intermediate frequencies, e.g., 500 Hz, it has been reported that electrophoresis can drive NPs to the surfaces, which results in EHD flow [22]. At higher frequencies when EHD flows dominate assembly, numerical calculations show that the rate of clustering is proportional to the square of the applied field and scales as $\sim\omega^{-2}$, with ω being the frequency, thus it is expected less clustering will occur at higher frequencies [26]. The cluster growth dynamics around Au seeds can be understood in terms of the double layer formation and free charge distribution [15,29]. At the high frequency regime (≥1000 Hz), changes in field polarity are too fast for counterions to uniformly redistribute around the particle surface [15]. Indeed the highest coverage of NP on the surface under all deposition conditions where EHD flow leads to clustering is observed at 500 Hz and the lowest coverage is observed at 1500 Hz.

The EHD flow velocity has also been reported to also be dependent on the particle's effective dipole orthogonal to the electrode surface [29]. For example, simulations on colloids near a conductive electrode have shown that the disturbance of the electric field potential and the slip velocity on the electrode's surface is greater around a dimer than a monomer [32]. Thus, as a few clusters form in these non-equilibrium conditions, there will be a stronger driving force for EHD flow around clusters versus monomers. As a result, once a cluster is nucleated there should be a tendency for growth into a larger cluster versus growth of a new cluster around a monomer. When the deposition time in the second step was increased to 4 min, the corresponding SEM images and statistical analysis is shown in Fig. S3. *2-dimensional* clusters grow larger at the longer deposition time for all frequencies and there is still a high surface coverage of monomers at 1500 Hz, further demonstrating the preference for growth of larger clusters than consumption of monomers at this frequency.

In order to investigate the origin of monomers after the second deposition step, we performed depositions of Au seeds at oscillatory potential of 5 V and frequency of 100 Hz and then a second deposition step of Ag NP was performed at the same potential with frequencies of

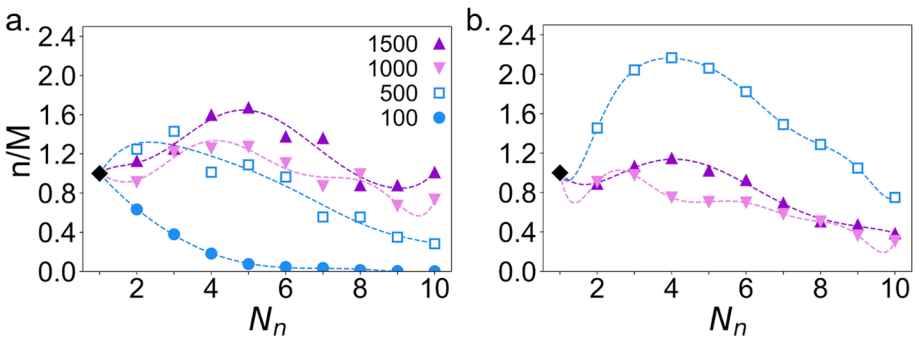

Fig. 3. Ratio of the number of particles in clusters of size n (N_n) to monomers (M) on the surface for **a)** single-step deposition and **b)** two-step deposition with the first step performed at 100 Hz and second at designated frequency in legend: 100 Hz (closed circles), 500 Hz (open squares), 1000 Hz (inverted triangles), and 1500 Hz (triangles). The oscillatory potential amplitude was 5 V in all cases.

500 Hz or 1500 Hz. SEM images in Fig. 4 acquired with a concentric backscattered detector (CBS) show compositional contrast where Au NP appear brighter than Ag NP due to a higher atomic number. These images were analyzed to determine the number of Au and Ag monomers remaining after the second deposition step and the number of clusters formed around Au NP versus Ag NP. Results are shown in Table 1. The data shows a nearly equal number of Au and Ag monomers on the surface after the second deposition at a frequency of 500 Hz. There is a slightly higher number of clusters nucleated from Au NP than from Ag NP when the second deposition is performed at 500 Hz. Thus, both electrophoresis and EHD flow appear to be driving forces for deposition at this frequency. In contrast, when the second deposition is performed at 1500 Hz, approximately 76% of the clusters formed during the second deposition originated from Au seeds. At the same time, Au seeds account for 85% of the remaining monomers. While some new monomers are deposited at 1500 Hz, this data indicates there is a preference for growth of existing clusters, once formed, versus a transition from monomer to cluster at a frequency of 1500 Hz. Thus, EHD appears to be a stronger driving force than electrophoresis for NP deposition at 1500 Hz.

Table 1
Statistical analysis of the fraction of Au or Ag monomers and clusters with Au and Ag NP versus clusters with only Ag NP observed in SEM images after EHD assembly of Au NP for 2 min with an oscillatory potential having an amplitude of 5 V and a frequency of 100 Hz, followed by a second deposition of Ag NP for 2 min at 500 Hz or 1500 Hz. SEM-CBS images analyzed had a field of view of approximately 30 μm^2.

Frequency	Monomers		Clusters	
	Au	Ag	Fraction with Au seed	Fraction with Ag only
500 Hz	45%	55%	62%	38%
1500 Hz	85%	15%	76%	24%

3.3. *In situ optical imaging*

SERS spectra is performed *in situ* to monitor the formation of clusters in response to EHD flow around Au nuclei. Before SERS imaging, Au NP functionalized with lipoic acid are assembled on a PS-*b*-PMMA coated Si electrode using the conditions to deposit isolated NP on the surface, i.e., potential amplitude of 5 V and frequency of 100 Hz, in order to *nucleate* EHD flow. After this first deposition step, a liquid cell is then formed with a 1.3 nM solution of Au NP functionalized with 4-mercaptobenzoic acid (4-MBA), a Raman reporter molecule, between the Si electrode with Au nuclei and an ITO coated glass slide as the counter electrode. An AC bias with an amplitude of 5 V and frequency of 500 Hz is applied to grow NP clusters with 4-MBA functionalized Au NP. As Au monomers are hypothesized to act as nucleation sites to generate EHD flow, one would expect the SERS intensity associated with 4-MBA to increase when plasmonic hotspots form in the nanogaps of clusters as they are formed. Our previous work has shown that EHD flow can lead to carbodiimide cross linking between carboxylic acid functional groups on NP ligands, leading to high SERS signal enhancements [2]. The laser beam is focused on the Si electrode and the SERS signal is monitored using an i-Raman Plus Portable Spectrometer with an excitation wavelength of 785 nm to measure cluster formation *in situ* as the potential is applied. As shown in Fig. 2a and d, the majority of the surface is covered by quadrumers and pentamers. Full-wave finite element simulations of 40 nm NP as a function of cluster size show the extinction maxima varies from 686 nm to 782 nm for dimers to octamers, respectively, for close packed clusters produced using EHD flow [2]. Fig. 5 shows that initially the SERS signal of 4-MBA vibrational modes is not observable from Au NP in colloidal solution. Two characteristic vibrational bands of 4-MBA, corresponding to the ν_{12} and ν_{8a} ring breathing modes at 1080 cm^{-1} and 1590 cm^{-1} [33], are observed after 10 s and the signal stabilizes after 20 s, indicating an appreciable level of clusters have formed on the surface.

Dissipative assembly in response to EHD flow was measured using confocal fluorescence spectroscopy *in situ* with the oscillatory potential cycled on and off on the same timescale of measured increased SERS intensity. The microfluidic channel, sandwiched between Si and ITO electrodes, is filled with an aqueous solution of Au NP, 1.3 nM, and nile red, 25 μM. Before fluorescence imaging, Au seeds functionalized with lipoic acid are deposited on Si substrates under conditions to deposit mainly monomers on the surface (Fig. 1a), except Si was coated with APTES to adhere NP to the surface via carbodiimide crosslinking chemistry using EDC/s-NHS. A thin carbon layer is then sputter coated on the Si electrode to mitigate electrostatic interactions between the NP in solution and the surface (Fig. S5). The laser beam, with a wavelength of 561 nm, is focused with an objective through the ITO coated slide onto the Si counter electrode. EHD flow is introduced by applying an oscillatory potential with an amplitude of 5 V and frequency of 500 Hz between the working and counter electrode, in on/off cycles of 20 s. Nile red has an absorption maximum at 552 nm and emission maximum at 633 nm. Previous studies have reported that metal enhanced fluorescence is maximum when localized surface plasmon resonance (LSPR) frequency of metal nanostructures is tuned to the emission spectra of the fluorophore [34]. In the fluorescence experimental setup the inter-nanoparticle spacing will be approximately 5 nm due to the carbon layer on Au seeds. The LSPR of a Au NP quadrumer with a similar inter-particle distance in aqueous solution was previously calculated to be approximately 600 nm for this system [1] and will redshift for larger clusters. The frequency of 500 Hz was selected for the second deposition step as this resulted in a high coverage of quadrumers and pentamers on the surface as observed in Figs. 2 and 3. Thus when nile red fluorophores are in the vicinity of Au NP clusters, the fluorescence emission may be

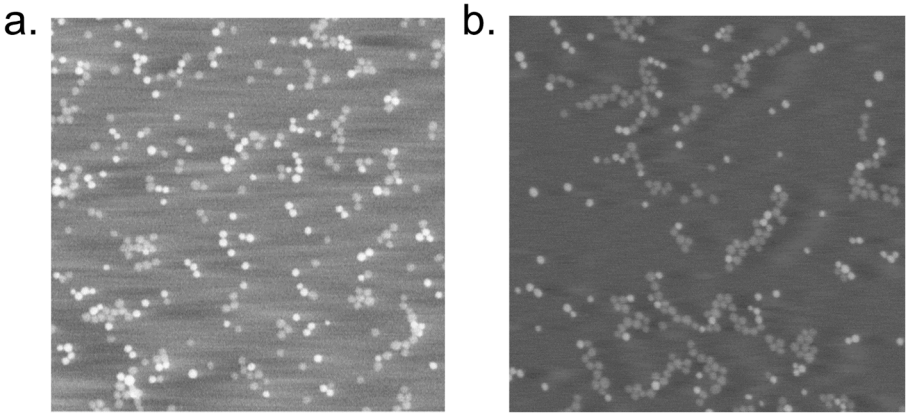

Fig. 4. Representative SEM-CBS images of surface with a field of view of 2 μm × 2 μm after EHD assembly of Au NP for 2 min with an oscillatory potential having amplitude of 5 V and frequency of 100 Hz, followed by a second deposition of Ag NP for 2 min at **a)** 500 Hz and **b)** 1500 Hz.

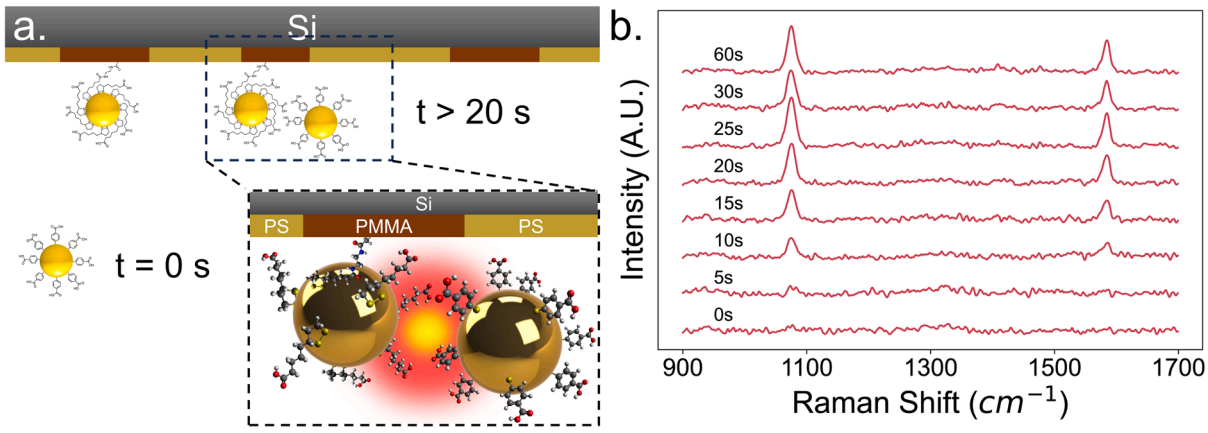

Fig. 5. a) Schematic of plasmonic hotspot formation as clusters form during EHD driven deposition of 4-MBA functionalized Au NP on surfaces with lipoic acid functionalized Au seeds on a PS-*b*-PMMA coated Si electrode. At $t = 0$ *s*, 4-MBA functionalized Au NP are suspended in solution and the Si surface has Au seeds. At $t > 0$ *s* an oscillatory potential with 5 V and 500 Hz is applied. **b)** SERS *in situ* spectral intensity at different deposition times. Stable signal intensity is observed at $t > 20$ *s*.

enhanced by more than an order of magnitude [34].

The average intensity of fluorescence signal as a function of time is shown in Fig. 6. The fluorescence signal increases and decreases in response to the oscillatory potential cycling on and off, respectively. The observed enhancements to the fluorescence signal when the AC field is on are consistent with metal enhancement of emission spectra of dye molecules; the resonance of clusters with NP nanogaps of distance of approximately 5–10 nm will overlap with dye emission frequency [35]. It appears that EHD flow drives the formation of clusters and therefore an increase in the average fluorescence intensity is observed when the oscillatory potential is on. In Fig. S6, the dissipative assembly behavior of NP via increases and decreases in fluorescence signal intensity is shown over the whole experimental investigation period, 12 cycles. Initially, there is a high background fluorescence signal but after the first 3 cycles the signal is reduced. This is attributed to fluorophores electrostatically adhered to the Si surface initially; similar work has shown an applied potential can reduce adhesion to the surface [36]. The fluorescence background intensity increases after 4 min of cycling, which we attribute to some NP irreversibly adhering to the electrode surface observed in similar systems [22]. Images from temporal videos of fluorescence intensity at specific time points by subtracting background image pixel intensity from the image pixel intensity observed when the oscillatory potential is on, and highlighted numerically in Fig. 6. The background intensity is determined when the oscillatory potential is off between the prior cycle and current cycle. Images are shown in Fig. 6 (i–iv); the full video is supplied in Supplementary Materials.

4. Conclusions

Colloidal NP deposited as isolated monomers on chemically patterned diblock copolymer on Si surfaces at low frequencies can serve as perturbations of electrode potential to nucleate EHD flow. As

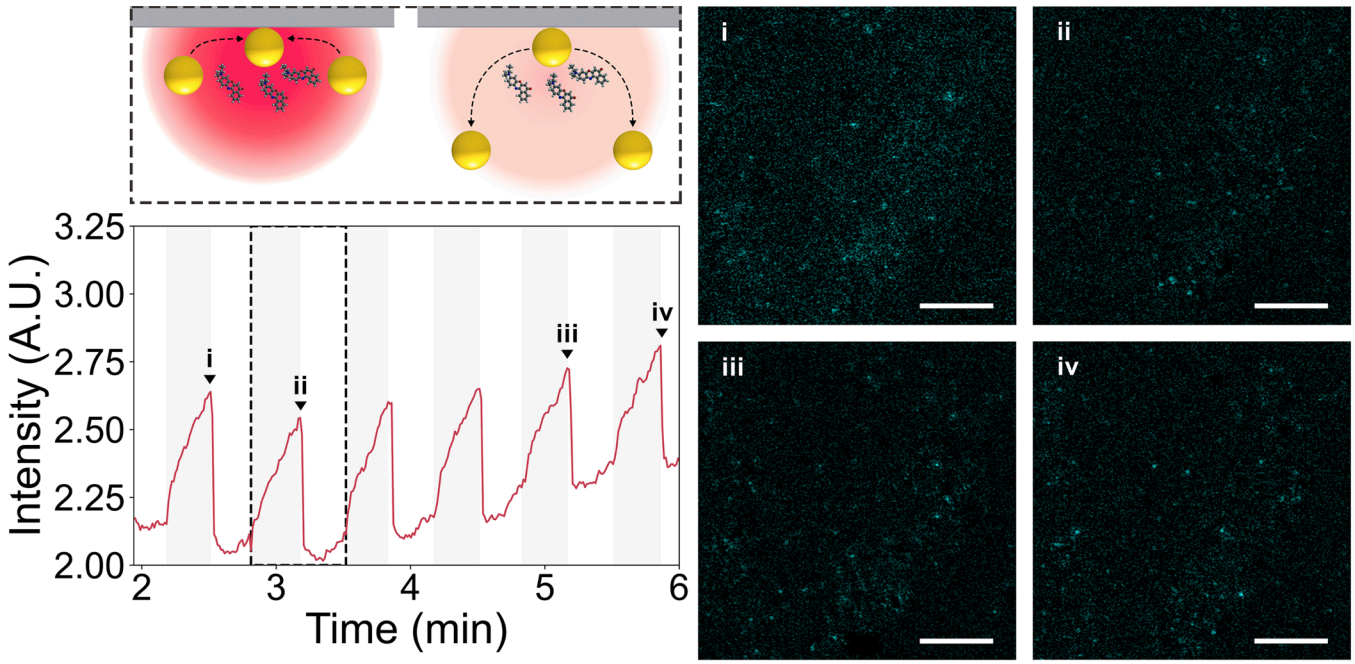

Fig. 6. Fluorescence intensity response to oscillatory potential: the temporal response of nile red average intensity in Au NP solution when the oscillatory electric field is cycled on and off in 20 s intervals. The laser is on for the duration of the experiment. The inset above is a schematic illustrating assembly and disassembly in response to the external stimuli. The images (i–iv) on the right are snapshots of background-subtracted video frames at time points indicated on the graph. All scale bars are 10 μm.

observed in SEM images, varying the frequency of the oscillatory potential can influence the assembly, where electrophoresis and EHD flow may contribute to resultant NP assemblies. At the lowest frequency investigated, 100 Hz, electrophoresis dominates deposition and single NP are deposited on the Si working electrode. At 500 Hz, smaller clusters with average size of trimers are formed and there appear to be contributions of both EHD flow and electrophoresis. At 1000 Hz and 1500 Hz, quadramers and pentamers, respectively, are observed most frequently. Changes in the cluster size distribution in the presence of Au monomer seeds associated with frequency provide further understanding of how frequency and effective dipole strength of the perturbation affect the rate of NP aggregation due to EHD flow. When using 100 Hz as the initial seed step to deposit Au monomers, serving as nuclei for EHD flow, a second deposition at an oscillatory frequency of 500 Hz was found to produce surfaces with 50% less monomers than in the single deposition while the average cluster size exhibited insignificant changes, 3.90 ± 0.97 versus 3.19 ± 0.77. Statistical analysis of SEM images of chemically crosslinked systems showed the highest overall NP coverage and the highest number of NP in clusters on surfaces was observed at 500 Hz. In comparison, a second step at 1000 Hz and 1500 Hz led to the formation of an increased number of dimers, trimers, and quadrumers while leaving many monomers. The appearance of a larger number of clusters of size four or smaller can be attributed to the presence of many perturbations (Au monomers) distributed across the surface at the beginning of the second deposition step. Numerical calculations predict that the EHD flow fields extend approximately 5 times the NP radius [26] on surfaces and thus the presence of distributed monomer seeds can lead to cluster assembly distributed across the surface. Furthermore, EHD velocity on surfaces scales with effective dipole strength and inversely with frequency [26]. Once clusters form, having a larger effective dipole than a monomer, there is a larger driving force for EHD flow around clusters versus monomer, explaining the large number of monomers remaining at higher frequencies. These results elucidate paths for future research of the parameter space affecting driving forces for assembly of NP on electrodes from colloids. When using *in situ* SERS for monitoring the assembly of 4-MBA functionalized Au NP, the resulting changes in spectral peak intensity is observed in approximately 10 s. With understanding of temporal scales for assembly, Au NP are demonstrated to serve as nanoantennas to report the occurrence of EHD flow driven dissipative assembly. Metal enhanced fluorescence monitors dissipative assembly where fluorescence intensity increases and decreases are observed when the oscillatory electric field is cycled on and off, respectively. The results show electrical driving forces can produce optically tunable surfaces and provide insights on how to tune cluster formation and resultant extinction frequency of dynamic surfaces.

Author contributions

R.R. designed all experiments and Z.G assisted in the design of confocal fluorescence measurements. H.W., H.P.H, and S.M. performed SEM characterization and EHD assembly experiments. H.W., H.P.H., and G.D.R. performed SEM characterization and statistical analysis of cluster distribution. H.W. and S.S. performed *in situ* confocal fluorescence. H.P.H performed the *in situ* Raman experiments. The manuscript was written by all authors. All authors have given approval to the final version of the manuscript.

CRediT authorship contribution statement

Hong Wei: Writing – review & editing, Writing – original draft, Investigation, Formal analysis. **Héctor Pascual-Herrero:** Writing – review & editing, Investigation, Formal analysis, Data curation. **Serxho Selmani:** Writing – original draft, Investigation, Formal analysis, Data curation. **Sebastian Marroquin:** Data curation, Investigation, Writing – review & editing. **Gabriel D. Reginato:** Writing – original draft, Investigation, Formal analysis, Data curation. **Zhibin Guan:** Writing – review & editing, Writing – original draft, Project administration, Funding acquisition, Formal analysis, Conceptualization. **Regina Ragan:** Writing – review & editing, Writing – original draft, Resources, Project administration, Methodology, Investigation, Funding acquisition, Formal analysis, Data curation, Conceptualization.

Declaration of competing interest

The authors declare that they have no known competing financial interests or personal relationships that could have appeared to influence the work reported in this paper.

Data availability

Data will be made available on request.

Acknowledgment

This research was primarily supported by the National Science Foundation Materials Research Science and Engineering Center program through the UC Irvine Center for Complex and Active Materials (DMR-2011967). The work was partially supported by the US Department of Energy, Office of Science, Basic Energy Sciences (DE-FG02-04ER46162, Z.G.) and the National Science Foundation (CHE-1904939, Z.G. and CBET-1926612, R.R.). The authors acknowledge the use of facilities and instrumentation at the UC Irvine Materials Research Institute (IMRI) supported in part by the National Science Foundation Materials Research Science and Engineering Center program through the UC Irvine Center for Complex and Active Materials (DMR-2011967). S.S. acknowledges support by an NSERC postdoctoral fellowship from the Research Council of Canada. H.P.H acknowledges support by the Balsells Fellowship program.

Appendix A. Supplementary data

Supplementary data to this article can be found online at https://doi.org/10.1016/j.jcis.2024.03.203.

References

[1] S.M. Adams, S. Campione, F. Capolino, R. Ragan, Directing cluster formation of Au nanoparticles from colloidal solution, Langmuir 29 (13) (2013) 4242–4251, https://doi.org/10.1021/la3051719.
[2] W.J. Thrift, C.Q. Nguyen, M. Darvishzadeh-Varcheie, S. Zare, N. Sharac, R. N. Sanderson, T.J. Dupper, A.I. Hochbaum, F. Capolino, M.J. Abdolhosseini Qomi, R. Ragan, Driving chemical reactions in plasmonic nanogaps with electrohydrodynamic flow, ACS Nano 11 (11) (2017) 11317–11329, https://doi.org/10.1021/acsnano.7b05815.
[3] A. Aubret, M. Youssef, S. Sacanna, J. Palacci, Targeted assembly and synchronization of self-spinning microgears, Nat. Phys. 14 (11) (2018) 1114–1118, https://doi.org/10.1038/s41567-018-0227-4.
[4] M. Mayer, M.J. Schnepf, T.A.F. König, A. Fery, Colloidal self-assembly concepts for plasmonic metasurfaces, Adv. Opt. Mater. 7 (1) (2019) 1800564, https://doi.org/10.1002/adom.201800564.
[5] J. Palacci, S. Sacanna, A.P. Steinberg, D.J. Pine, P.M. Chaikin, Living crystals of light-activated colloidal surfers, Science 339 (6122) (2013) 936–940, https://doi.org/10.1126/science.1230020.
[6] F. Nan, F. Han, N.F. Scherer, Z. Yan, Dissipative self-assembly of anisotropic nanoparticle chains with combined electrodynamic and electrostatic interactions, Adv. Mater. 30 (45) (2018) 1803238, https://doi.org/10.1002/adma.201803238.
[7] J. Yan, M. Han, J. Zhang, C. Xu, E. Luijten, S. Granick, Reconfiguring active particles by electrostatic imbalance, Nat. Mater. 15 (10) (2016) 1095–1099, https://doi.org/10.1038/nmat4696.
[8] T. Hueckel, G.M. Hocky, S. Sacanna, Total synthesis of colloidal matter, Nat. Rev. Mater. 6 (11) (2021) 1053–1069, https://doi.org/10.1038/s41578-021-00323-x.
[9] B. Liebchen, A.K. Mukhopadhyay, Interactions in active colloids, J. Phys. Condens. Matter 34 (8) (2021) 083002, https://doi.org/10.1088/1361-648X/ac3a86.
[10] Y. Ma, C. Zagar, D.J. Klemme, D. Sikdar, L. Velleman, Y. Montelongo, S.-H. Oh, A. R. Kucernak, J.B. Edel, A.A. Kornyshev, A tunable nanoplasmonic mirror at an electrochemical interface, ACS Photonics 5 (11) (2018) 4604–4616, https://doi.org/10.1021/acsphotonics.8b01105.
[11] Y. Ma, D. Sikdar, A. Fedosyuk, L. Velleman, D.J. Klemme, S.-H. Oh, A.R. J. Kucernak, A.A. Kornyshev, J.B. Edel, Electrotunable nanoplasmonics for

amplified surface enhanced Raman spectroscopy, ACS Nano 14 (1) (2020) 328–336, https://doi.org/10.1021/acsnano.9b05257.
[12] Y. Montelongo, D. Sikdar, Y. Ma, A.J.S. McIntosh, L. Velleman, A.R. Kucernak, J. B. Edel, A.A. Kornyshev, Electrotunable nanoplasmonic liquid mirror, Nat. Mater. 16 (11) (2017) 1127–1135, https://doi.org/10.1038/nmat4969.
[13] J.R. Maestas, F. Ma, N. Wu, D.T. Wu, Electric-field-driven assembly of dipolar spheres asymmetrically confined between two electrodes, ACS Nano 15 (2) (2021) 2399–2412, https://doi.org/10.1021/acsnano.0c04939.
[14] M. Trau, D.A. Saville, I.A. Aksay, Assembly of colloidal crystals at electrode interfaces, Langmuir 13 (24) (1997) 6375–6381, https://doi.org/10.1021/la970568u.
[15] M. Goel, A. Singh, A. Bhola, S. Gupta, Size-tunable assembly of gold nanoparticles using competitive AC electrokinetics, Langmuir 35 (24) (2019) 8015–8024, https://doi.org/10.1021/acs.langmuir.8b03963.
[16] W.D. Ristenpart, I.A. Aksay, D.A. Saville, Assembly of colloidal aggregates by electrohydrodynamic flow: kinetic experiments and scaling analysis, Phys. Rev. E 69 (2) (2004) 021405, https://doi.org/10.1103/PhysRevE.69.021405.
[17] M.-G. Song, K.J.M. Bishop, A.O. Pinchuk, B. Kowalczyk, B.A. Grzybowski, Formation of dense nanoparticle monolayers mediated by alternating current electric fields and electrohydrodynamic flows, J. Phys. Chem. C 114 (19) (2010) 8800–8805, https://doi.org/10.1021/jp1008253.
[18] A.A. Harraq, B.D. Choudhury, B. Bharti, Field-induced assembly and propulsion of colloids, Langmuir 38 (10) (2022) 3001–3016, https://doi.org/10.1021/acs.langmuir.1c02581.
[19] C.S. Dutcher, T.J. Woehl, N.H. Talken, W.D. Ristenpart, Hexatic-to-disorder transition in colloidal crystals near electrodes: rapid annealing of polycrystalline domains, Phys. Rev. Lett. 111 (12) (2013) 128302, https://doi.org/10.1103/PhysRevLett.111.128302.
[20] M. Rath, J. Weaver, M. Wang, T. Woehl, pH-Mediated aggregation-to-separation transition for colloids near electrodes in oscillatory electric fields, Langmuir 37 (31) (2021) 9346–9355, https://doi.org/10.1021/acs.langmuir.1c00671.
[21] A. Zöttl, H. Stark, Modeling active colloids: from active Brownian particles to hydrodynamic and chemical fields, Annu. Rev. Condens. Matter Phys. 14 (1) (2023) 109–127, https://doi.org/10.1146/annurev-conmatphys-040821-115500.
[22] A. Ferrick, M. Wang, T.J. Woehl, Direct visualization of planar assembly of plasmonic nanoparticles adjacent to electrodes in oscillatory electric fields, Langmuir 34 (21) (2018) 6237–6248, https://doi.org/10.1021/acs.langmuir.8b00992.
[23] R.K. Grötsch, C. Wanzke, M. Speckbacher, A. Angı, B. Rieger, J. Boekhoven, Pathway dependence in the fuel-driven dissipative self-assembly of nanoparticles, J. Am. Chem. Soc. 141 (25) (2019) 9872–9878, https://doi.org/10.1021/jacs.9b02004.
[24] Z. Chai, A. Childress, A.A. Busnaina, Directed assembly of nanomaterials for making nanoscale devices and structures: mechanisms and applications, ACS Nano 16 (11) (2022) 17641–17686, https://doi.org/10.1021/acsnano.2c07910.
[25] J.H. Choi, S.M. Adams, R. Ragan, Design of a versatile chemical assembly method for patterning colloidal nanoparticles, Nanotechnology 20 (6) (2009) 065301, https://doi.org/10.1088/0957-4484/20/6/065301.
[26] W.D. Ristenpart, I.A. Aksay, D.A. Saville, Electrohydrodynamic flow around a colloidal particle near an electrode with an oscillating potential, J. Fluid Mech. 575 (2007) 83–109, https://doi.org/10.1017/S0022112006004368.
[27] W.D. Ristenpart, P. Jiang, M.A. Slowik, C. Punckt, D.A. Saville, I.A. Aksay, Electrohydrodynamic flow and colloidal patterning near inhomogeneities on electrodes, Langmuir 24 (21) (2008) 12172–12180, https://doi.org/10.1021/la801419k.
[28] A.D. Hollingsworth, D.A. Saville, A broad frequency range dielectric spectrometer for colloidal suspensions: cell design, calibration, and validation, J. Colloid Interface Sci. 257 (1) (2003) 65–76, https://doi.org/10.1016/S0021-9797(02)00029-2.
[29] W.D. Ristenpart, I.A. Aksay, D.A. Saville, Electrically driven flow near a colloidal particle close to an electrode with a faradaic current, Langmuir 23 (7) (2007) 4071–4080, https://doi.org/10.1021/la062870l.
[30] X. Yang, S. Johnson, N. Wu, The impact of stern-layer conductivity on the electrohydrodynamic flow around colloidal motors under an alternating current electric field, Adv. Intell. Syst. 1 (8) (2019) 1900096, https://doi.org/10.1002/aisy.201900096.
[31] M. Trau, D.A. Saville, I.A. Aksay, Field-induced layering of colloidal crystals, Science 272 (5262) (1996) 706–709, https://doi.org/10.1126/science.272.5262.706.
[32] A. Atay, A. Beşkök, B. Çetin, DC-electrokinetic motion of colloidal cylinder(s) in the vicinity of a conducting wall, Electrophoresis 43 (12) (2022) 1263–1274, https://doi.org/10.1002/elps.202100266.
[33] A. Michota, J. Bukowska, Surface-Enhanced Raman Scattering (SERS) of 4-mercaptobenzoic acid on silver and gold substrates, J. Raman Spectrosc. 34 (1) (2003) 21–25, https://doi.org/10.1002/jrs.928.
[34] F. Tam, G.P. Goodrich, B.R. Johnson, N.J. Halas, Plasmonic enhancement of molecular fluorescence, Nano Lett. 7 (2) (2007) 496–501, https://doi.org/10.1021/nl062901x.
[35] D. Lu, S. Hou, S. Liu, Q. Xiong, Y. Chen, H. Duan, Amphiphilic Janus magnetoplasmonic nanoparticles: pH-triggered self-assembly and fluorescence modulation, J. Phys. Chem. C 126 (35) (2022) 14967–14975, https://doi.org/10.1021/acs.jpcc.2c03753.
[36] T.J. Woehl, K.L. Heatley, C.S. Dutcher, N.H. Talken, W.D. Ristenpart, Electrolyte-dependent aggregation of colloidal particles near electrodes in oscillatory electric fields, Langmuir 30 (17) (2014) 4887–4894, https://doi.org/10.1021/la4048243.